

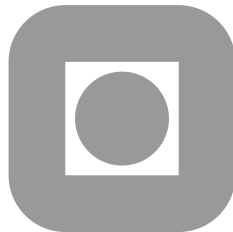
NORGES TEKNISK-NATURVITENSKAPELIGE
UNIVERSITET

**Conservation of phase space properties using
exponential integrators on the cubic Schrödinger
equation**

by

Håvard Berland, Alvaro L. Islas and Constance Schober

PREPRINT
NUMERICS NO. 1/2006



NORWEGIAN UNIVERSITY OF
SCIENCE AND TECHNOLOGY
TRONDHEIM, NORWAY

This report has URL

<http://www.math.ntnu.no/preprint/numerics/2006/N1-2006.pdf>

Address: Department of Mathematical Sciences, Norwegian University of Science and
Technology, N-7491 Trondheim, Norway.

Conservation of phase space properties using exponential integrators on the cubic Schrödinger equation

Håvard Berland* Alvaro L. Islas[†] Constance M. Schober[‡]

The cubic nonlinear Schrödinger (NLS) equation with periodic boundary conditions is solvable using Inverse Spectral Theory. The “nonlinear” spectrum of the associated Lax pair reveals topological properties of the NLS phase space that are difficult to assess by other means. In this paper we use the invariance of the nonlinear spectrum to examine the long time behavior of exponential and multisymplectic integrators as compared with the most commonly used split step approach. The initial condition used is a perturbation of the unstable plane wave solution, which is difficult to numerically resolve. Our findings indicate that the exponential integrators from the viewpoint of efficiency and speed have an edge over split step, while a lower order multisymplectic is not as accurate and too slow to compete.

1 Introduction

Exponential integrators have been popular in recent literature and they seem especially attractive in PDE settings as a means of easily obtaining high order explicit schemes without step size restrictions for the time-integration. The notable property of exponential integrators is the use a splitting of the problem into a linear part, possibly rendering the problem stiff, and a nonlinear part. The linear part is treated exactly, in an attempt to ameliorate temporal step size restrictions imposed by possible stiffness inherent in the PDE problem. However, experience with exponential integrators on long time scales for various PDEs with a complicated phase space structure is not abundant. This paper examines whether exponential integrators are a viable alternative for the time integration of PDEs, by comparing them with two other classes of time-integrators and by using the NLS equation as a benchmark problem.

The NLS equation is completely integrable with a rich phase space structure (i.e. stable as well as unstable solutions with homoclinic orbits). Typically the performance of an integrator has been determined by examining the preservation of global invariants such as energy and momentum. The nonlinear spectrum of the associated Lax pair of the PDE provides a detailed description of the phase space and is invariant in time. Following [17],

*Department of Mathematical Sciences, Norwegian University of Science and Technology, N-7491 Trondheim, Norway, Havard.Berland@math.ntnu.no

[†]Department of Mathematics, University of Central Florida, Orlando, FL32816-1364, USA, aislas@mail.ucf.edu, cschober@mail.ucf.edu

we monitor the spectrum to assess how well the phase space is preserved by the various integrators. Section 2 outlines the necessary properties of the inverse spectral theory.

For Hamiltonian PDEs possessing a multisymplectic structure (symplectic in both space and time), multisymplectic integrators preserve exactly a discrete version of the multisymplectic structure [10]. For quadratic Hamiltonians, multisymplectic integrators preserve the local conservation laws exactly. Even though this is not the case for the NLS equation, multisymplectic integrators were shown to provide improved resolution of the local conservation laws and dynamical invariants [16, 17]. Compared to classical integrators (Runge–Kutta), multisymplectic integrators exhibited less drift in the conservation laws over long time periods [17]. We include an implicit second order multisymplectic integrator for comparison with the exponential integrators and it is found to be the most computationally demanding integrator among those tested. Whether improved preservation of the structural and geometric properties of the PDE by multisymplectic integrators justifies their additional computational cost remains an open question.

Section 3 gives the necessary details of the spectral space discretization, which will be equivalent for all schemes included in this study. In Section 3.2 exponential integrators are presented in a format including the majority of known exponential integrators, and specifications of the exponential integrators used are given in coefficient function tableaus. We restrict our attention to explicit exponential integrators to facilitate speed and ease of implementation, and test the two integrators CFREE4 and LAWSON4. The implementation has used the MATLAB package described in [7] directly. A fourth order split step scheme obtained by Yoshida’s technique is included for comparison, as it is, in many ways, related to exponential integrators and it is also used fairly extensively in the physics community. We only included a multisymplectic integrator of order two as, even at this order, it turned out to be computationally more intensive than the other integrators. Our final criteria for comparing integrators is based on accuracy obtained for fixed CPU time, and thus it makes sense to compare integrators with differing asymptotic order.

The numerical results are given in Section 4 where we examine how well the most critical features of the nonlinear spectrum are preserved. Knowledge of the properties of the nonlinear spectrum makes it possible to give simple criteria for determining whether a numerical result is acceptable or not. We present results in table form and conclude that among our integrators, CFREE4 seems to be the most reliable and CPU effective choice for our problem.

The nonlinear Schrödinger equation

The periodic focusing nonlinear Schrödinger (NLS) equation

$$u_t = iu_{xx} + i2|u|^2u, \tag{1}$$

$u(x + D, t) = u(x, t)$, is an infinite dimensional integrable Hamiltonian system with Hamiltonian

$$H(u, u^*) = \int_0^D (|u_x|^2 - |u|^4) dx. \tag{2}$$

The (complex) solution $u(x, t)$ represents the slow space-time evolution of the envelope of a carrier signal, and has important applications in nonlinear optics, deep water waves and also plasma physics. The wave equation (1) bears its name because it corresponds to the quantum Schrödinger equation with $2|u|^2$ as the potential.

An important physical prediction of the NLS equation is the Benjamin–Feir or modulational instability for periodic boundary conditions [4]. An example of this is provided by

the plane wave solution,

$$u(x, t) = ae^{2i|a|^2t}. \quad (3)$$

which has M linearly unstable modes with growth rates $\sigma_n^2 = \mu_n^2(\mu_n^2 - 4a^2)$, $\mu_n = 2\pi n/D$, provided

$$0 < (\pi n/D)^2 < |a|^2 \quad (4)$$

is satisfied (the number M of unstable modes is the largest integer satisfying $0 < M < |a|D/\pi$). That is, the plane wave is unstable with respect to long wavelength perturbations.

In the numerical experiments we consider multi-phase solutions whose initial data is obtained by perturbing the plane wave solution,

$$u(x, 0) = a \left(1 + \epsilon e^{i\psi} \cos(\mu_n x) \right), \quad (5)$$

where $a = \frac{1}{2}$, $\mu_n = \frac{2\pi n}{D}$ and $D = 4\sqrt{2}\pi$ is the length of the spatial domain. Typically, the strength of the perturbation ϵ is chosen to be 0.1, $\psi = 0$ and $n = 1$. For the given spatial length D , the plane wave has two unstable modes, thereby the initial condition is coined the two-mode case. Increasing the spatial period results in more unstable modes, making the problem numerically harder.

2 The inverse spectral method

In [28], the NLS equation (1) was shown by Zakharov and Shabat to be completely integrable (with infinite sequences of commuting flows and common conservation laws) and solvable by inverse scattering theory for rapidly decreasing initial data on the infinite line. Special solutions such as solitons, which are localized wave packets (envelope solutions for the NLS equation) that survive collisions with one another, were proven to exist in this case. More generally, inverse spectral theory provides a method, the analog of the whole-line inverse scattering theory, for solving the NLS equation on periodic domains. Its, Krichever and Kotlarov used inverse spectral theory and methods of algebraic geometry to obtain N -phase solutions of the periodic NLS equation, expressible in terms of Riemann theta functions [18, 20, 3].

2.1 Lax pair and characterization of the spectrum

The inverse scattering and spectral methods may be viewed as a generalization of Fourier methods for solving linear PDEs. Briefly, the complete integrability of the NLS equation is established by using the associated Lax pair of linear operators defined by [28]:

$$\mathcal{L}^{(x)}\phi = 0 \quad \text{and} \quad \mathcal{L}^{(t)}\phi = 0, \quad (6)$$

where

$$\mathcal{L}^{(x)} = \begin{pmatrix} \frac{d}{dx} + i\lambda & -u \\ u^* & \frac{d}{dx} - i\lambda \end{pmatrix} \text{ and } \mathcal{L}^{(t)} = \begin{pmatrix} \frac{d}{dt} + i[2\lambda^2 - |u|^2] & -2\lambda u - iu_x \\ 2\lambda u^* - iu_x^* & \frac{d}{dt} - i[2\lambda^2 - |u|^2] \end{pmatrix} \quad (7)$$

The coefficients $u(x, t)$ are periodic in x , $u(x + D, t) = u(x, t)$, λ is the spectral parameter, and ϕ is the eigenfunction. The NLS equation arises as the solvability or compatibility condition for these operators, i.e., $\phi_{xt} = \phi_{tx}$ if and only if $u(x, t)$ satisfies the NLS equation (1).

The first step in solving the NLS equation is to calculate the direct spectral transform of the initial data, i.e. to determine the spectrum of $\mathcal{L}^{(x)}$, which is analogous to calculating the Fourier coefficients in Fourier theory. Next, time evolution is performed on the ‘‘spectral

data" using $\mathcal{L}^{(t)}$. Finally the inverse spectral transform is calculated in order to recover the waveform at a later time.

The direct spectral transform and its inverse provide a one-to-one correspondence between solutions of the NLS equation and the spectral data. The spectral data consists of two types of spectrum of $\mathcal{L}^{(x)}$; the periodic eigenvalues λ_j and the Dirichlet eigenvalues μ_j (to be defined below). The direct spectral transform consists of computing (λ_j, μ_j) from $u(x, t)$. A fundamental property is that the periodic eigenvalues λ_j are invariants of the NLS flow whereas the Dirichlet spectrum flows in both x and t . The time dependence of $\mu_j(x, t)$ is generated by $\mathcal{L}^{(t)}$ and is equivalent to the dynamics of the NLS flow since $\mathcal{L}^{(x)}$ and $\mathcal{L}^{(t)}$ are compatible. The inversion formula for N -phase solutions of the NLS is given by the trace formula [18]:

$$\frac{i u_x}{u} = \sum_{j=1}^{2N} \lambda_j - 2 \sum_{j=1}^{N-1} \mu_j.$$

For periodic potentials the spectrum is obtained using Floquet theory. This spectral analysis is similar to that of the time-independent Hill's operator, with the main difference that $\mathcal{L}^{(x)}$ is not self-adjoint. The spectrum of u ,

$$\sigma(u) = \left\{ \lambda \in \mathbf{C} \mid \mathcal{L}^{(x)}\phi = 0, |\phi| \text{ bounded } \forall x \right\}, \quad (8)$$

can be expressed in terms of the transfer matrix $M(x + D; u, \lambda)$ across a period, where $M(x; u, \lambda)$ is a fundamental solution matrix of the Lax pair (7). Introducing the Floquet discriminant $\Delta(u, \lambda) = \text{Trace}[M(x + L; u, \lambda)]$, one obtains

$$\sigma(u) = \{ \lambda \in \mathbf{C} \mid \Delta(u, \lambda) \in \mathbf{R}, -2 \leq \Delta(u, \lambda) \leq 2 \}. \quad (9)$$

The distinguished points of the periodic/antiperiodic spectrum are where $\Delta(u, \lambda_j) = \pm 2$, and are categorized as

- (a) Simple points $\{ \lambda_j^s \mid \frac{d\Delta}{d\lambda} \neq 0 \}$,
- (b) Double points $\{ \lambda_j^d \mid \frac{d\Delta}{d\lambda} = 0, \frac{d^2\Delta}{d\lambda^2} \neq 0 \}$.

The Floquet discriminant functional $\Delta(u, \lambda)$ is invariant under the NLS flow and encodes the infinite family of constants of motion of the NLS (parametrized by the λ_j 's). While the λ_j 's are equivalent to a set of invariant action variables, the μ_j 's (which are the zeros of the M_{12} entry of the transfer matrix and are not invariant) provide the conjugate angle variables.

The Floquet spectrum (9) of a generic NLS potential consists of the entire real axis plus additional curves (called bands) of continuous spectrum in the complex plane which terminate at the simple points λ_j^s . N -phase solutions are those with a finite number of bands of continuous spectrum. Double points can be thought of as the coalescence of two simple points and their location is particularly significant. The order and location of the λ_j completely determine the spatial structure and nonlinear mode content of NLS solutions as well as the dynamical stability as follows [12, 13]:

- (a) Simple points correspond to stable active degrees of freedom.
- (b) Double points label all additional potentially active degrees of freedom.

Real double points correspond to stable inactive (zero amplitude) modes. Complex double points correspond to the unstable active modes and parametrize the associated homoclinic orbits.

The N -phase quasiperiodic solutions of the NLS equation have the form [3, 18, 20],

$$u(x, t) = u_0 e^{i(k_0 x - \omega_0 t)} \frac{\Theta(\mathbf{W}^-|\tau)}{\Theta(\mathbf{W}^+|\tau)}, \quad (10)$$

where Θ is the Riemann theta function, $\mathbf{W}^\pm = (W_1^\pm, \dots, W_N^\pm)$, and the phases evolve according to $W_j^\pm = (\kappa_j x + \Omega_j t + \theta_j^\pm)$. The external phase as well as the wavenumbers κ_j and frequencies Ω_j are expressible in terms of algebraic-geometric data including the branch points of the associated Riemann surface (namely, the simple points λ_j^s of the Floquet spectrum). The entire x and t dependence of an N -phase solution is captured by ODEs for the μ_j 's. Essentially these ODEs linearize via the classical Abel–Jacobi map associated with the Riemann surface. The phases W_j^\pm in the action-angle description of these solutions are the images of $\mu_j(x, t)$ under the Abel–Jacobi map.

In terms of the NLS phase space, the values of the actions λ_j fix a particular level set. The level set defined by u is then given by, $\mathcal{M}_u \equiv \{v \mid \Delta(v, \lambda) = \Delta(u, \lambda), \lambda \in \mathbf{C}\}$. Typically, \mathcal{M}_u is an infinite dimensional stable torus. However, the NLS phase space also contains degenerate tori which may be unstable. If a torus is unstable, its invariant level set consists of the torus and an orbit homoclinic to the torus. These invariant level sets, consisting of an unstable component, are represented, in general, by complex double points in the spectrum [13].

In our experiments we implement the first step of the inverse spectral method and appeal to the invariance of the λ_j 's to evaluate the ability of the various numerical schemes to preserve the NLS phase space structure. The nonlinear spectrum for the Lax pair (7) is computed numerically using Fortran software at each timevalue of the solution. In our case, only the λ_j 's where $\Delta = \pm 2$ are necessary. The discriminant function Δ is obtained by a direct nonlinear spectral transform, solving the overdetermined system of ODEs (in the variable x) given by the Lax pair for the given numerical solution $u(x, t)$. The zeros of $\Delta = \pm 2$ are then obtained with a root solver using Muller's method as in [21]. The spectrum itself is calculated with an accuracy of $\mathcal{O}(10^{-8})$ which is sufficient for our results.

2.2 Perturbation of the plane wave

The simplest example of an N -phase solution of the NLS equation is the plane wave solution (3). In this case, the Floquet discriminant is given by $\Delta(a, \lambda) = 2 \cos(\sqrt{a^2 + \lambda^2} D)$ and thus the spectrum consists of the entire real axis and the band $[-ia, ia]$. At $\pm ia$ there is a pair of simple periodic/antiperiodic eigenvalues and there is an infinite sequence of double points,

$$\lambda_j^2 = (j\pi/D)^2 - a^2 \quad (11)$$

for $j \in \mathbf{Z}$, of which $2\lfloor aD/\pi \rfloor = 2M$ are pure imaginary double points and the remaining are real. The condition for a complex double point is exactly the condition for a mode to be linearly unstable (compare with (4)). However, in contrast to inverse spectral theory, linear analysis does not provide any answers to what happens to the solution on a long time-scale.

When $a = 0.5$ and $D = 4\sqrt{2}\pi$ in (3), $M = 2$ and λ_1 and λ_2 are complex double points (since the spectrum is symmetric with respect to the real axis we restrict our consideration to $\text{Im } \lambda \geq 0$). It is difficult in advance to predict the time of failure using only physical data or a few global constants. For the family of initial data (5), as the energy levels are varied slightly there are alternating windows of stable and unstable tori. As a consequence, we have found that the λ_j 's, which determine the geometry of the level sets, are the significant quantities to preserve [17].

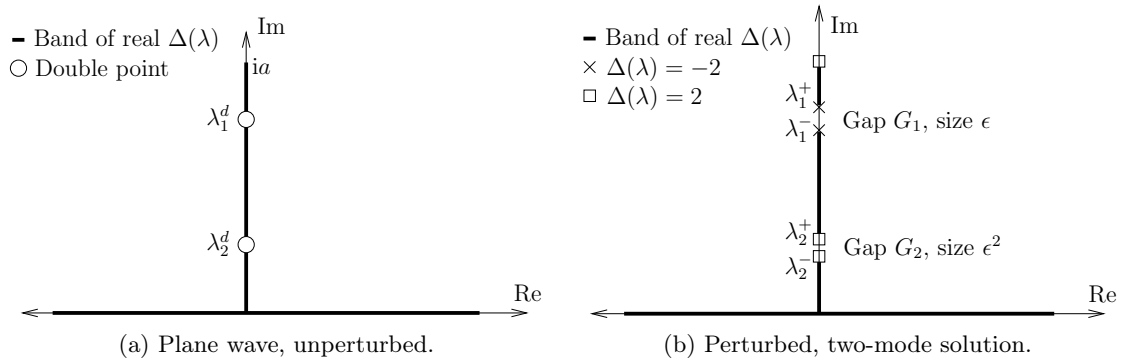


Figure 1: The spectrum (9) for (a) the plane wave (3) and (b) the perturbed plane wave data (5). The perturbation of strength ϵ opens up the two double points of the plane wave spectrum (a) and yields the perturbed spectrum (b) with two gaps corresponding to two semi-stable modes in the solution (see Figure 2). Real double points are not shown.

Assuming $u = u^{(0)} + \epsilon u^{(1)} + \dots$, $\lambda = \lambda^{(0)} + \epsilon \lambda^{(1)} + \dots$, and $\phi = \phi^{(0)} + \epsilon \phi^{(1)} + \dots$, the spectrum of initial data (5) can be calculated via perturbation analysis. Substituting these expansions into (7), the $\lambda_j^{(0)}$ are given by (11) and the corrections at $\mathcal{O}(\epsilon)$ are [2]

$$\left(\lambda_j^{(1)}\right)^2 = \begin{cases} \frac{a^2}{16\lambda_j^2} \left(e^{-i\phi} - \frac{1}{a^2} (j\pi/D + \lambda_j)^2 e^{i\phi} \right) \\ \quad \cdot \left(e^{-i\phi} - \frac{1}{a^2} (-j\pi/D + \lambda_j)^2 e^{i\phi} \right) & j = n \\ 0 & j \neq n \end{cases} \quad (12)$$

At $\mathcal{O}(\epsilon)$ there is a correction only to the double point $\lambda_j^{(0)}$, ($j = n$), which resonates with the perturbation. The other double points do not experience an $\mathcal{O}(\epsilon)$ correction.

The behavior of the correction $\lambda_j^{(1)}$, ($j = n$), depends on whether the double point $\lambda_j^{(0)}$ is real or imaginary:

$$\left(\lambda_j^{(1)}\right)^2 = \begin{cases} -\frac{a^2}{4\lambda_j^2} \sin(\phi + \theta) \sin(\phi - \theta) & \text{for } \lambda_j \text{ imaginary} \\ -\frac{a^2}{8\lambda_j^2} [\cos 2\phi + 1 - 2(j\pi/D)^2/a^2] & \text{for } \lambda_j \text{ real} \end{cases}$$

where $\tan \theta = \text{Im}(\lambda_j)D/(j\pi)$. Since initial data (5) is for a solution even in x , the spectrum has an additional symmetry with respect to the imaginary axis. This is reflected in the correction $\lambda_j^{(1)}$ which, for imaginary double points, is either real, zero or pure imaginary [2] depending on the choice of ψ in the perturbed potential, i.e. imaginary double points can split into either crosses or gaps in the spectrum. This is a realization of the saddle structure of the real part $\Delta(u, \lambda_j)$ when λ_j is imaginary. More generally, if the potential is noneven in x , the correction $\lambda_j^{(1)}$ is fully complex and the double point can split in any direction, yielding an asymmetric version of a gap state.

For real double points, the correction $\lambda_j^{(1)}$ can only be imaginary. Gaps cannot appear on the real axis in the spectrum of $\mathcal{L}^{(x)}$. Hence the situation with real double points is very different from that of imaginary double points. Splitting of real double points only introduces additional degrees of freedom into the spatial structure but does not introduce an instability as homoclinic manifolds are not associated with them. At the next order only the double points λ_j , ($j = 2n$), experience an $\mathcal{O}(\epsilon^2)$ -splitting. A full determination of the splitting at higher order is given in [2] and in the non-even case in [1].

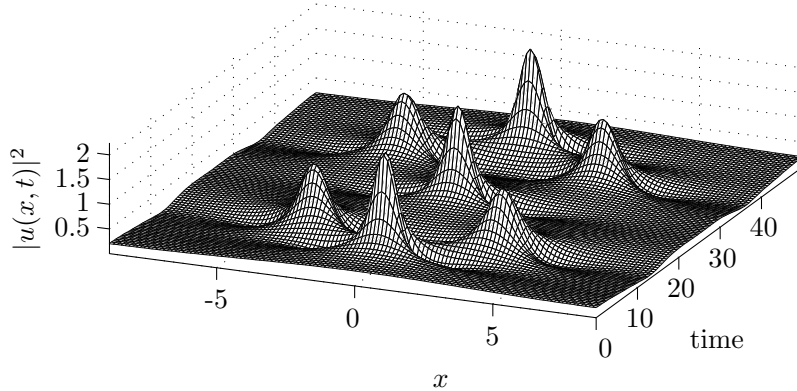


Figure 2: The surface $|u(x, t)|^2$ of the nonlinear Schrödinger equation with initial condition (5). The center mode around $x = 0$ corresponds to gap G_1 in Figure 1b, and the second mode appearing around $x = \pm 3$ in the $|u(x, t)|^2$ -plot corresponds to gap G_2 in Figure 1b.

The Floquet spectrum for initial data (5), with $\psi = 0$ and $n = 1$ is shown in Figure 1b. The corrections to λ_1 and λ_2 , as determined by (12), are pure imaginary and gaps G_1 and G_2 open in the spectrum with sizes of order ϵ and ϵ^2 , respectively [2]. The double point λ_j splits into λ_j^\pm and the gap $G_j = \lambda_j^+ - \lambda_j^-$. The first gap corresponds to the center mode in Figure 2 and from λ_1^\pm the spatial and temporal frequencies of the mode are determined. Similarly λ_2^\pm (corresponding to the smaller gap of size ϵ^2) determine the wave number and frequency of the second mode which appears symmetrically on both sides. If the ratio of the two temporal frequencies is a rational number, the initial condition will recur in finite time.

3 Numerical integrators

3.1 Space discretization

The instability of the NLS equation which we are examining occurs only for periodic boundary condition, thus it is reasonable to restrict our attention to spectral spatial discretizations making use of the fast Fourier transform. The spatial resolution is equivalent for all of the schemes considered, so the differences in performance are attributable to the time integrators.

Let

$$\hat{u}(k, t) = \mathcal{F}(u(x, t)) = \frac{1}{D} \int_{-D/2}^{D/2} u(x, t) e^{-\nu_k x} dx$$

with $k \in \mathbf{Z}$ and $\nu_k = \frac{2\pi i}{D} k$ be the Fourier transform of $u(x, t)$. The inverse Fourier transform is

$$u(x, t) = \mathcal{F}^{-1}(\hat{u}(k, t)) = \sum_{k=-\infty}^{\infty} \hat{u}(k, t) e^{\nu_k x}.$$

In Fourier space, equation (1) then takes the form of an infinite system of first order ODEs

$$\begin{aligned} \hat{u}_t(k, t) &= i\nu_k^2 \hat{u}(k, t) + 2i |\mathcal{F}^{-1}(\hat{u}(k, t))|^2 \hat{u}(k, t) & k \in \mathbf{Z}, \quad t \geq 0 \\ \hat{u}(k, 0) &= \mathcal{F}(u(x, 0)) \end{aligned} \quad (13)$$

The spatial discretization now consists of truncating (13) to $N_{\mathcal{F}}/2 \leq k \leq N_{\mathcal{F}}/2 - 1$, and the resulting system of dimension $N_{\mathcal{F}}$ is then solved by the integrators mentioned below.

3.2 Exponential integrators

Exponential integrators are a class of integrators that emerged from an improved ability in numerical software to compute the matrix exponential in a reasonable amount of time. Recent developments [5, 11, 15, 22] have yielded an abundance of possibilities with regards to choice of scheme (see for instance [7] and the accompanying source code for a listing). In this study we examine the performance of the class of exponential integrators; thus, the particular choice of exponential integrator is of less importance. After numerous initial numerical tests, we have chosen CFREE4 as “the” exponential integrator in this report. It gives the best overall performance for our problem as measured by the global error and the preservation of invariants over long integration intervals.

An s -stage explicit exponential integrator of Runge–Kutta type for the system of ordinary differential equations

$$\dot{y}(t) = Ly(t) + N(y, t), \quad y(0) = y_0 \in \mathbf{R}^n \quad (14)$$

where L is linear and $N(y, t)$ is a (possibly) nonlinear function, is the procedure

$$Y_i = \sum_{j=1}^s a_{ij}(hL) hN(Y_j, t_0 + c_j h) + \exp(c_i hL) y_0 \quad (15a)$$

$$y_1 = \sum_{i=1}^s b_i(hL) hN(Y_i, t_0 + c_i h) + \exp(hL) y_0 \quad (15b)$$

in which Y_i , $i = 1, \dots, s$, are internal stages and y_1 is the final approximation of $y(t_1) = y(t_0 + h)$. This format extends the format for Runge–Kutta schemes in that the coefficients a_{ij} and b_i are now analytic functions in the matrix L .

In short, the main properties of an exponential integrator are (i) when the linear part L is zero, we recover the *underlying* Runge–Kutta-scheme, and (ii) when $N \equiv 0$, exponential integrators compute the exact solution. The coefficient functions $a_{ij}(z)$ and $b_i(z)$ ($z = hL$) are usually listed in a tableau similar to the Butcher tableau for Runge–Kutta schemes. For CFREE4, the functions are

$$\begin{array}{c|ccc|c} 0 & & & 1 \\ \frac{1}{2} & \frac{1}{2}\varphi_{1,2} & & e^{z/2} \\ \frac{1}{2} & & \frac{1}{2}\varphi_{1,2} & e^{z/2} \\ 1 & \frac{1}{2}\varphi_{1,2}(e^{z/2} - 1) & \varphi_{1,2} & e^z \\ \hline & \frac{1}{2}\varphi_1 - \frac{1}{3}\varphi_{1,2} & \frac{1}{3}\varphi_1 & \frac{1}{3}\varphi_1 - \frac{1}{6}\varphi_1 + \frac{1}{3}\varphi_{1,2} \\ & & & e^z \end{array} \quad (16)$$

where

$$\varphi_\ell(z) = \frac{1}{(\ell - 1)!} \int_0^1 e^{(1-\theta)z} \theta^{\ell-1} d\theta, \quad \ell = 1, 2, \dots \quad (17)$$

and

$$\varphi_{i,j} = \varphi_i(c_j z), \quad i = 1, \dots \text{ and } j = 1, \dots, s. \quad (18)$$

For $\ell = 1, 2, 3$ (and for $z \neq 0$) the functions are

$$\varphi_1(z) = \frac{e^z - 1}{z}, \quad \varphi_2(z) = \frac{e^z - z - 1}{z^2}, \quad \text{and} \quad \varphi_3(z) = \frac{e^z - z^2/2 - z - 1}{z^3}.$$

There is a singularity at $z = 0$ that could potentially lead to cancellation errors for small time steps. In order to avoid this in our experiments, these so called φ functions are

evaluated by scaling the argument z , using a Padé approximant of φ_ℓ , and squaring the result. Details for this are presented in [7] and further analyzed in [8, 19].

Stiff order analysis of exponential integrators was introduced as an analytical tool in [15] which addresses the convergence of exponential integrators for semi-linear parabolic partial differential equations. To obtain order p convergence in that case, independently of spatial resolution, stiff order p for the exponential integrator is required. Stiff order conditions represent an additional set of order conditions, including the classical order conditions as a special case. The CFREE4 scheme is only of stiff order 2, but still outperformed the other schemes in the initial study, including expensive schemes with high stiff order, though only marginally in some cases.

The report [6] is a study of two fourth order exponential integrators on the nonlinear Schrödinger equation, one Lawson integrator with stiff order 1, and ETD4RK from [11] with stiff order 2. Some effects (exhibited through order reduction) were attributable to low stiff order of the Lawson integrators, possibly also connected to preservation of fixed points, a condition equivalent to stiff order 2. Given sufficient spatial smoothness of the nonlinear function, and sufficient smoothness of the initial condition, high stiff order seemed less important. Also in [6], connections between the Lawson type and split step integrators are indicated, and it is in this respect that we include the Lawson integrator of order 4 but stiff order 1, LAWSON4, with tableau

$$\begin{array}{c|ccc|c}
 0 & & & & 1 \\
 \frac{1}{2} & \frac{1}{2}e^{z/2} & & & e^{z/2} \\
 \frac{1}{2} & & \frac{1}{2} & & e^{z/2} \\
 1 & & & e^{z/2} & e^z \\
 \hline
 & \frac{1}{6}e^z & \frac{1}{3}e^{z/2} & \frac{1}{3}e^{z/2} & \frac{1}{6} \\
 & & & & e^z
 \end{array} . \tag{19}$$

Both CFREE4 and LAWSON4 reduce to the same classical fourth order Runge–Kutta scheme when the linear part is zero.

In the spectral space discretization, the matrix L in (14) for (13) becomes diagonal with elements

$$L_{kk} = i\nu_k^2 = -ik^2/8, \quad k = -N_{\mathcal{F}}/2, \dots, N_{\mathcal{F}}/2 - 1. \tag{20}$$

The nonlinear function N in (14) becomes

$$N(\hat{u}(k, t), t) = 2i \left| \mathcal{F}^{-1}(\hat{u}(k, t)) \right|^2 \hat{u}(k, t). \tag{21}$$

Our implementation uses fixed step sizes for all schemes, and as the linear part is time-independent, the functions e^{ciz} and $\varphi_{i,j}$ are computed only at time zero of the integration and cached for the subsequent integration steps. Thus, the cost of evaluating the exponential and the φ functions are amortized over long integration intervals.

3.3 Second order multisymplectic spectral

The multisymplectic formulation for the nonlinear Schrödinger equation was introduced in [10], as an integrator being symplectic in both time and space. Multisymplectic integrators preserve exactly a discrete version of multisymplecticity. If the Hamiltonian function $S(z)$ is space and time independent, the PDE will possess local energy and momentum conservation laws. In addition, if $S(z)$ is quadratic in z , a multisymplectic integrator will preserve exactly these local conservation laws and, in the periodic case, the associated global conservation laws.

Although the Hamiltonian for the NLS equation is space and time independent, it is not quadratic and thus only multisymplecticity is exactly conserved in this case. Nevertheless, multisymplectic integrators have been reported to preserve the conservation laws better than classical Runge–Kutta schemes [17].

We will first show the multisymplectic formulation for a finite difference discretization of a PDE, then we see how it simplifies when using a spectral discretization in space.

Equation (1) can be written in multisymplectic form by letting $u = p+iq$ and augmenting the phase space with the variables $v = p_x$ and $w = q_x$. The system obtained is

$$\begin{aligned} q_t - v_x &= 2(p^2 + q^2)p \\ -p_t - w_x &= 2(p^2 + q^2)q \\ p_x &= v \\ q_x &= w \end{aligned} \tag{22}$$

A Hamiltonian PDE is defined as multisymplectic if it can be written in the form

$$Mz_t + Kz_x = \nabla_z S(z)$$

where M and K are skew-symmetric matrices, and S is a smooth function of the state variable z . Formulation (22) of the nonlinear Schrödinger equation is multisymplectic provided

$$z = \begin{pmatrix} p \\ q \\ v \\ w \end{pmatrix}, \quad M = \begin{pmatrix} 0 & 1 & 0 & 0 \\ -1 & 0 & 0 & 0 \\ 0 & 0 & 0 & 0 \\ 0 & 0 & 0 & 0 \end{pmatrix}, \quad K = \begin{pmatrix} 0 & 0 & -1 & 0 \\ 0 & 0 & 0 & -1 \\ 1 & 0 & 0 & 0 \\ 0 & 1 & 0 & 0 \end{pmatrix},$$

and $S(z) = \frac{1}{2}((p^2 + q^2)^2 + v^2 + w^2)$.

The multisymplectic conservation law is

$$\omega_t + \kappa_x = 0 \tag{23}$$

where ω and κ are alternating forms

$$\omega(U, V) = \langle MU, V \rangle = V^T MU \quad \text{and} \quad \kappa(U, V) = \langle KU, V \rangle = V^T KU \tag{24}$$

for two solutions, U and V , of the variational equation associated to the PDE (22) [10]. An integrator of the system (22) is multisymplectic if and only if a discretized version of (23) is preserved exactly.

The centered cell discretization [10] is a centered difference approximation in space to (22), and implicit midpoint in space, which can be proven to be a multisymplectic scheme. However, in our periodic case, the finite difference discretization in space is inferior to a spectral space discretization, and thus, it has not been included in the numerical tests in this report.

Instead, the centered cell discretization is modified to use a spectral discretization in space. Approximation of space differentiation can be seen as multiplication by the spectral differentiation matrix \mathcal{D} [14],

$$\frac{du}{dx} \approx \mathcal{D}\{u_k\}, \quad u_k \approx u(x_k), \quad \mathcal{D} = \begin{cases} (-1)^{j-k} \frac{\pi}{D} \cot \frac{\pi}{D}(x_j - x_k) & \text{if } j \neq k \\ 0 & \text{if } j = k \end{cases} \tag{25}$$

Replacing all space derivatives in (22) with spectral differentiation using \mathcal{D} , and modifying the multisymplectic conservation law (23) accordingly, in [17] the authors prove that this together with implicit midpoint in time yields a multisymplectic scheme for the nonlinear Schrödinger equation. We denote this scheme MSSPECTRAL2. The implicit equation at each time step is solved numerically using a simplified Newton iteration.

3.4 Fourth order split step scheme

Split step schemes have been used for a long time for integrating the nonlinear Schrödinger equation in physical applications. In our context, [25] is an early reference to the type of scheme. Taha and Ablowitz [24] give an extensive survey of the prime integrators for the numerical solution of the nonlinear Schrödinger equation, and conclude that Tappert's split step Fourier scheme [25] is in most cases superior to the other schemes considered. The paper [26] investigates numerical aspects of the basic first order split step Fourier method using linearization techniques.

For the split step Fourier method to be comparable to the fourth order exponential integrators used, we first construct a second order scheme by using a Strang splitting technique [23] and the same splitting as for exponential integrators. Let $\Phi_{\text{RK4C}}^h(y(t_0))$ be the approximation to $y(t_0 + h)$ produced by Kutta's classical fourth order scheme for the problem $\dot{y}(t) = N(y, t)$. Then a Strang splitting scheme for (14) is

$$\Phi_{\text{SS2}}^h(y_0) = \Phi_{\text{RK4C}}^{h/2} \circ \exp(hL) \circ \Phi_{\text{RK4C}}^{h/2}(y_0) \quad (26)$$

with L and N given by (20) and (21). Then we use Yoshida's formula

$$\Phi_{\text{SS4}}(y_0) = \Phi_{\text{SS2}}^{c_1 h} \circ \Phi_{\text{SS2}}^{c_0 h} \circ \Phi_{\text{SS2}}^{c_1 h}(y_0) \quad (27)$$

to construct a fourth order split step scheme from the second order Strang scheme, where $c_0 = \frac{-2^{1/3}}{2-2^{1/3}}$ and $c_1 = \frac{1}{2-2^{1/3}}$ [27]. Scheme (27) will be denoted SPLITSTEP4 in the remainder of this paper.

SPLITSTEP4 is picked as a representative and well-studied scheme within the class of split step schemes for the nonlinear Schrödinger equation. However, recently symplectic partitioned Runge–Kutta schemes have been constructed for the nonlinear Schrödinger equation which maybe could outperform the SPLITSTEP4 scheme used here, as reported in [9]. In further studies, these new split step schemes should also be compared to exponential integrators.

4 Numerical results

The NLS (1) equation with a perturbed plane wave solution as the initial condition (5) has been integrated with various choices of the spatial discretization parameter $N_{\mathcal{F}}$ and the temporal step size h . Our aim is to determine the time length for which the numerical solution is valid, where the validity is determined by how well the nonlinear spectrum is preserved, and thereby judge the chosen integrators. Table 1 indicates the length of time for which the numerical solution was accepted according to criteria based entirely on the nonlinear spectrum and constitutes the main result from this work.

4.1 Preservation of nonlinear spectrum

The spectrum of the NLS equation is invariant in time, but the truncation errors incurred by the numerical schemes result in numerical solutions that can be viewed as the exact solutions of corresponding perturbed equations, for which the spectra evolve in time. Thus, the positions of the single/double points and the bands of real discriminant $\Delta(u, \lambda)$, computed by software briefly described in Section 2.1, will in general vary in time. It has been customary in similar studies to monitor conservation of momentum, energy and norm. These three quantities are expressible in terms of the nonlinear spectrum, but alone fail to describe all the properties of the spectrum.

	$h = 10^{-1}$	$h = 10^{-2}$	$h = 10^{-3}$	$h = 10^{-4}$
CFREE4	6.9 ⁽¹⁾	6.9 ⁽¹⁾	6.9 ⁽¹⁾	6.9 ⁽¹⁾
LAWSON4	6.9 ⁽¹⁾	6.9 ⁽¹⁾	6.9 ⁽¹⁾	6.9 ⁽¹⁾
SPLITSTEP4	6.7 ^(1,2)	6.9 ⁽¹⁾	6.9 ⁽¹⁾	6.9 ⁽¹⁾
MSSPECTRAL2	26.2 ⁽¹⁾	6.9 ⁽¹⁾	6.9 ⁽¹⁾	6.9 ⁽¹⁾

(a) $N_{\mathcal{F}} = 64$

	$h = 10^{-1}$	$h = 10^{-2}$	$h = 10^{-3}$	$h = 10^{-4}$
CFREE4	90.1 ⁽¹⁾	157.9 ⁽¹⁾	157.9 ⁽¹⁾	157.9 ⁽¹⁾
LAWSON4	6.8 ⁽²⁾	157.9 ⁽¹⁾	157.9 ⁽¹⁾	157.9 ⁽¹⁾
SPLITSTEP4	7 ^(1,2)	2049 ^(r)	157.9 ⁽¹⁾	157.9 ⁽¹⁾
MSSPECTRAL2	5.9 ⁽²⁾	207.8 ⁽¹⁾	158 ⁽¹⁾	157.9 ⁽¹⁾

(b) $N_{\mathcal{F}} = 128$

	$h = 10^{-1}$	$h = 10^{-2}$	$h = 10^{-3}$	$h = 10^{-4}$
CFREE4	90.3 ⁽¹⁾	3165 ^(r)	> 10000	> 10000
LAWSON4	6.7 ⁽²⁾	1891 ^(r)	> 10000	> 10000
SPLITSTEP4	7.1 ^(1,2)	2400 ^(r)	> 10000	> 10000
MSSPECTRAL2	5.9 ⁽²⁾	207.6 ⁽²⁾	1426 ^(r)	> 500

(c) $N_{\mathcal{F}} = 256$

	$h = 10^{-1}$	$h = 10^{-2}$	$h = 10^{-3}$	$h = 10^{-4}$
CFREE4	90.3 ⁽¹⁾	3166 ^(r)	> 10000	> 10000
LAWSON4	6.7 ⁽²⁾	1993 ^(r)	> 10000	> 10000
SPLITSTEP4	7.1 ^(1,2)	907.4 ^(r)	1479 ^(r)	> 10000
MSSPECTRAL2	5.9 ⁽²⁾	109.8 ⁽²⁾	1426 ^(r)	n/a

(d) $N_{\mathcal{F}} = 512$

Table 1: Time until numerical solution fails. Symbols next to numbers denote reason for failure.

The initial condition is a perturbation of an unstable state, and the numerical challenge is to balance near the border of this instability. We allow for discrepancies that are small enough not to excite any of the unstable modes, or said differently, we avoid *topological* changes to the spectral configuration.

If the gap size becomes zero (gap closure) we obtain a degenerate double point, as in the plane wave solution $\epsilon = 0$, Figure 1a, and the solution may then undergo a homoclinic crossing, entering a completely different state. A typical scenario after a gap closure is that eigenvalues at the end of the bands λ_j^\pm obtain a nonzero real part and the mode enters a “cross” state. This corresponds to the solution having different spatial structure. Spatial symmetry is also typically lost as the modes may start to drift spatially. As symmetry is not enforced in the numerical solutions, accumulation of non-symmetric round-off errors may eventually ruin the numerical solution. In the non-symmetric (non-even) case, it is seen in [1] that the real part of the eigenvalues may grow without being initiated by a homoclinic crossing. The gap sizes and the magnitude of the real part of the single points have therefore been used as the main indicators of the validity of the numerical solution.

The numerical solution at time T is accepted given that the topological properties of the spectrum have remained unchanged for $0 \leq t \leq T$. Let

$$G_j(t) = \lambda_j^+(t) - \lambda_j^-(t), \quad j = 1, 2, \quad (28)$$

denote the gap (complex valued) G_j at time t with reference to Figure 1a.

We monitor the deviations in the spectrum λ_j^\pm , examining the real and imaginary components independently. The precise requirements used are

$$\begin{aligned} \frac{1}{100} |\operatorname{Im} G_j(0)| < |\operatorname{Im} G_j(t)| < 100 |\operatorname{Im} G_j(0)| & \quad \text{for } j = 1, 2, \\ |\operatorname{Re} G_j(0)| < 5 \cdot 10^{-5}. & \end{aligned} \quad (29)$$

The smallest t for which one of these requirements are not met in a given scenario is printed in Table 1. The specific numbers 100 and $5 \cdot 10^{-5}$ have been chosen to reveal the significant differences between the integrators in preserving the vital features of the phase space structure, that is, allowing everything but *topological* changes in the spectrum. The numbers must also be comparable to the eigenvalue accuracy of the spectrum computation, which in our case has been $\mathcal{O}(10^{-8})$. Also note that $|\operatorname{Im} G_j(t)|$ never reached its upper limit before the solution was invalidated by the other requirements in our experiments.

Based on the numerical solutions and the accompanying spectra produced, we find that the nonlinear spectrum evolves in four different ways.

- (1) Gap 1 closes ($|\operatorname{Im} G_1| \approx 0$). Subsequently, $|\operatorname{Re} G_1|$ is nonzero. The numerical solution is said to “cross” a homoclinic orbit and enter a different state, often with the center mode spatially shifted half the domain length. This is exemplified in Figure 3.
- (2) Gap 2 closes ($|\operatorname{Im} G_2| \approx 0$). Subsequently, $|\operatorname{Re} G_2|$ is nonzero. Gap 2 corresponds to the antiperiodic mode appearing on both sides of the center mode, and also experiences spatial shift during gap closure and homoclinic crossing. This is exemplified in Figure 4.
- (1,2) Both gaps close. This is similar to the two cases above, but here both gaps close during the time span defined by one peak of a mode. In the scenarios included here, this has been the onset of computational chaos in the numerical solution. This is exemplified in Figure 5.
- (r) $|\operatorname{Re} G_2|$ becomes nonzero, without any gap closures. This only happens on long time scales, and is due to accumulation of non-symmetric round-off errors. The sign of λ_2^+ and λ_2^- is always different, and the sign of λ_2^+ determines the direction (right or left) the corresponding mode will travel in phase space. The real extent determine the speed of spatial drift. In some of the cases, this case is followed by $|\operatorname{Re} G_1|$ becoming non-zero as well. This is exemplified in Figure 6.

It is evident from the data in Table 1 that sufficient spatial resolution is a first prerequisite for a valid long-time computation. Using only $N_{\mathcal{F}} = 64$, G_1 closes during the first peak of the center mode for all integrators independent of temporal step size h , except for MSSPECTRAL2, which fails at the second center mode peak.

Increasing spatial accuracy to $N_{\mathcal{F}} = 128$ one can integrate for a longer period of time, but still, for most configurations G_1 closes early. Of special interest is the exceptional result of SPLITSTEP4 for $h = 10^{-2}$, where gap closures are avoided but the accumulation of non-symmetric round-off error eventually grows large enough to destroy the solution. However, finer experiments indicated that there is a small window for h in which better spectrum preservation is achieved for this integrator. In general, for $N_{\mathcal{F}} = 128$ and $h \leq 0.01$, there are no significant differences in the performance of the various schemes.

At $N_{\mathcal{F}} = 256$ the spatial resolution is sufficient to reveal differences in the time-integration. If $h \leq 0.001$, all of the schemes are able to integrate for as long as we tested.

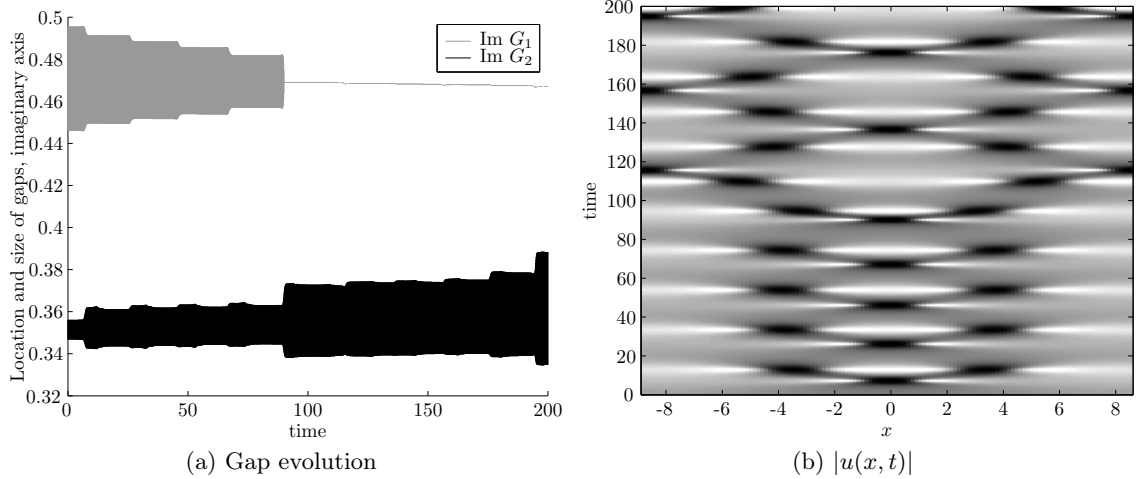


Figure 3: Example of failure due to closure of G_1 for CFREE4, $h = 0.1$, $N_{\mathcal{F}} = 128$. At each time slice, the points λ_j^{\pm} are located at the end of the bars drawn, and the length of the bar denotes the extent of the gap. In the surface plot to the right, a darker tone indicates higher value, compare with Figure 2.

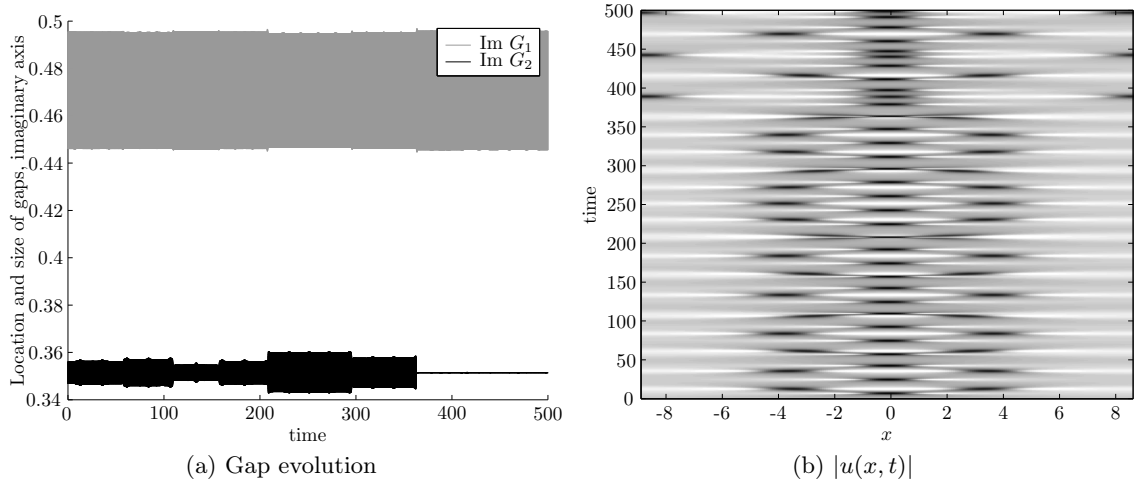


Figure 4: Example of failure due to closure of G_2 . MSSPECTRAL2, $h = 0.01$, $N_{\mathcal{F}} = 256$.

CFREE4, LAWSON4, and SPLITSTEP4 all suffer from a growth in the real part for $h = 0.01$, but all are good for smaller step sizes. This non zero real part is visible in the surface plots as a spatial drift in the modes. MSSPECTRAL2 behaves well for $N_{\mathcal{F}} = 128$ for $h = 0.01$ but suffers from a growth in the real part for $h = 0.001$ where the other integrators do not experience as much growth. Due to the computational complexity, MSSPECTRAL2 has not been computed over as long time intervals as the others.

Not much is gained by increasing the spatial resolution to $N_{\mathcal{F}} = 512$, but one should note that this turns out to be more difficult for SPLITSTEP4, as we observe a spatial drift for $h = 0.001$ which does not occur at $N_{\mathcal{F}} = 256$. Further, the validity time is smaller for the higher resolution of $N_{\mathcal{F}} = 512$ for $h = 0.01$ and $h = 0.001$. It is only in this case that SPLITSTEP4 is significantly less appealing than the exponential integrators.

The experiments have all been run on Intel Pentium IV processors using MATLAB Release 14SP3 (Version 7.1). During the experiments we noted that in some scenarios Release 14SP3 gave different numerical results (usually slightly worse) than those obtained with

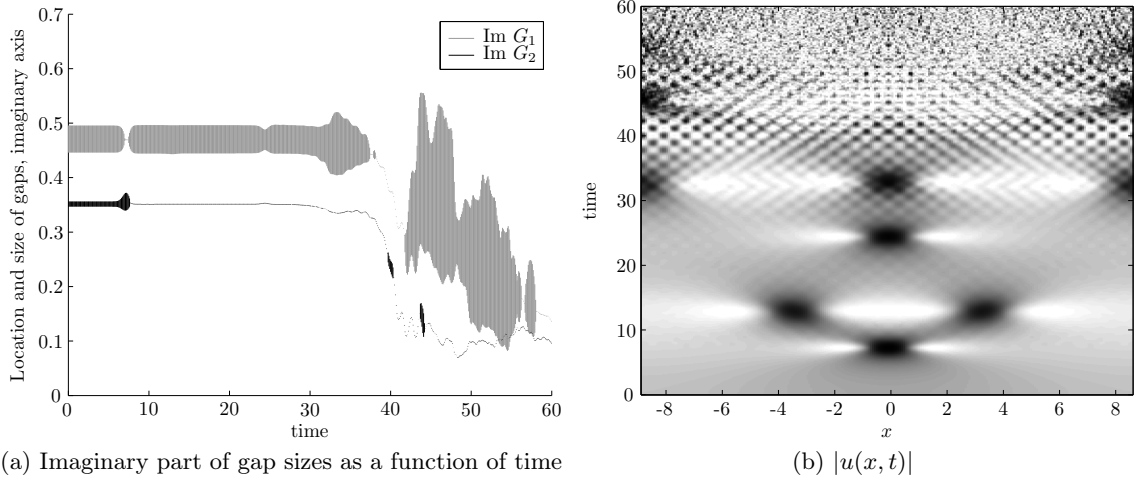


Figure 5: Example of failure due to closure of G_1 and G_2 . SPLITSTEP4, $h = 0.01$, $N_{\mathcal{F}} = 256$. Development of computational chaos as observed here is typical for SPLITSTEP4.

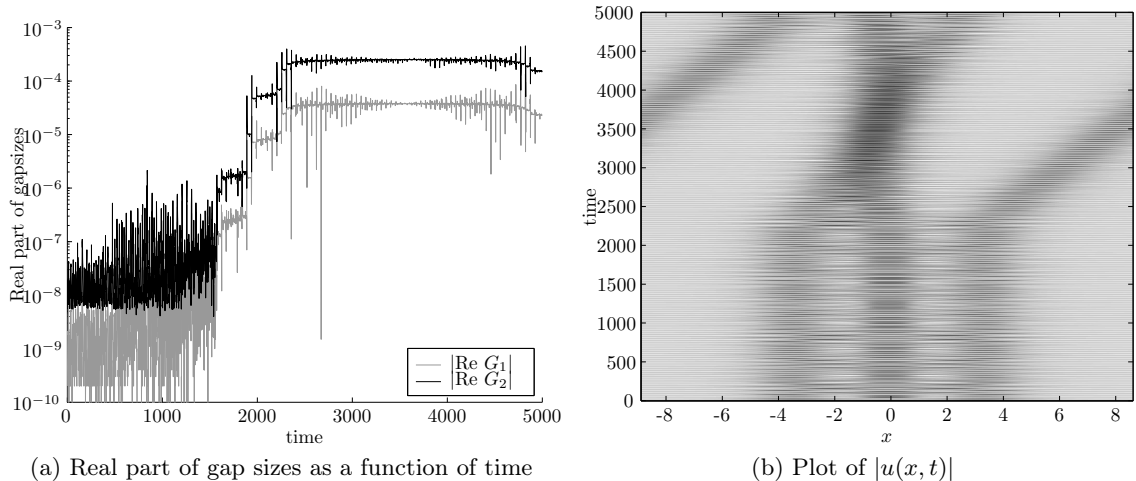


Figure 6: Example of failure due to breakdown of symmetry, nonzero real part of single points λ_j^{\pm} . LAWSON4, $h = 0.01$, $N_{\mathcal{F}} = 256$. The imaginary extent of the gaps is well preserved in this case.

the same code and processor but using MATLAB Release 13 (Version 6.5). Effects due to round-off errors, as in this case with the growth in real part, is more prone to differ between releases of MATLAB, and also possibly differ with the specific hardware used.

4.2 Computational time

Measuring computational complexity is a difficult task, and the results in this section should only be taken as an indication. Time has been measured by the built-in `cputime` command in MATLAB. The exponential integrators have been implemented using the EX-PINT-package, and thus it incurs an overhead in that the package is designed modularly. A specific exponential integrator applied to a specific problem could be hand-crafted and would result in speedup for that exponential integrator and problem. In the exponential integrators, the time step is constant, which facilitates caching of the exponential function of the linear part and the φ functions. This is automatically taken care of by the

Integrator	$h = 0.1$	$h = 0.01$	$h = 0.001$
CFREE4	1020.4	1089.9	1091.2
LAWSON4	913.2	1119.2	1114.1
SPLITSTEP4	423.7	435.4	443.7
MSSPECTRAL2	69.7	102.1	115.5

(a) 64 Fourier modes

Integrator	$h = 0.1$	$h = 0.01$	$h = 0.001$
CFREE4	593.5	649.4	656.8
LAWSON4	630.9	674.3	678.2
SPLITSTEP4	211.2	215.4	226.5
MSSPECTRAL2	2.6	4.3	5.1

(b) 256 Fourier modes

Table 2: Number of integration steps per CPU second, 2.4GHz Intel Pentium IV

EXPINT-package, and is also crucial for an exponential integrator implementation of this type. The multisymplectic code is to a certain degree already tailored to the problem in question, but nevertheless, this code is probably the one which could gain the most relative performance increase from optimization and tuning in the root solver. However, it is not believed that any optimization performed on the code for MSSPECTRAL2 will make any substantial changes to the results obtained in this work.

Table 2 contains timing data measured in steps per second with varying time step and integrator. Exponential integrators should not be significantly dependent on time step, but the multisymplectic integrator is, due to easier solvability of the root problem for decreasing h .

5 Discussion

In this study, we have used inverse spectral method as a tool to determine whether a solution obtained numerically for different integrators and discretization parameters is acceptable. We have integrated initial conditions ϵ -close to unstable states, which makes the problem hard numerically, as truncation errors from the space discretization, truncation errors from time-integration and round-off errors in the computer may eventually force the numerical solution to enter another state and then diverge from the exact solution. An unacceptable solution in this context means that the spectrum of the solution has changed topologically from its initial state, possibly through homoclinic crossings.

We tested the integrators CFREE4, LAWSON4, SPLITSTEP4, and MSSPECTRAL2, the last one being a second order implicit multisymplectic integrator. In short, CFREE4 was shown to exhibit the most stable properties in terms of being able to integrate for a long time avoiding topological changes to the spectrum. In addition, it is the computationally fastest integrator for given discretization parameters.

The two exponential integrators outperformed the other schemes. CFREE4 appeared slightly more stable than LAWSON4, perhaps attributable to higher stiff order, or its preservation of fixed points of the differential equation. SPLITSTEP4, being related to LAWSON4, was comparable, but performed less reliably than the exponential integrators. Its performance was not monotone in terms of spatial and temporal resolution.

The multisymplectic integrator MSSPECTRAL2, which gave good results on the one-mode case in [17], was not able to match the other schemes in this study, both in terms of

preservation of spectrum and especially in terms of computational complexity.

The nature and computational demands of these experiments dictated that all possibilities could not be tested, and not all scenarios could be integrated until breakdown. The experiments could have been performed with additional configurations, possibly revealing more information on for instance SPLITSTEP4's peak performance on $N_{\mathcal{F}} = 128$ and $h = 0.01$. Also, there is a multitude of alternative exponential integrators that probably would have performed along the lines of CFREE4, at least those with stiff order at least 2. The conclusion here is more to advocate the use of exponential integrators, more than to advocate the use of the specific CFREE4 scheme.

6 Acknowledgements

Håvard Berland is grateful for the opportunity to stay at Department of Mathematics, University of Central Florida, Orlando US, with Dr. Constance Schober and Dr. Alvaro Islas, during autumn 2005.

References

- [1] M. J. Ablowitz, B. M. Herbst, and C. M. Schober. Computational chaos in the nonlinear schrödinger equation without homoclinic crossings. *Physica A*, 228:212–235, 1996.
- [2] M. J. Ablowitz and C. M. Schober. Effective chaos in the nonlinear schrödinger equation. *Contemporary Mathematics*, 172:253–268, 1994.
- [3] E. D. Belokolos, A. I. Bobenko, V. Z. Enol'skii, A. R. Its, and V. B. Matveev. *Algebraic-Geometric Approach to Nonlinear Integrable Equations*. Springer series in nonlinear dynamics. Springer-Verlag, Berlin, 1994.
- [4] T. B. Benjamin and J. E. Feir. The disintegration of wave trains on deep water. *J. Fluid Mech.*, 27(3):417–430, 1967.
- [5] H. Berland, B. Owren, and B. Skaflestad. B -series and order conditions for exponential integrators. *SIAM J. Numer. Anal.*, 43(4):1715–1727, 2005.
- [6] H. Berland, B. Owren, and B. Skaflestad. Solving the nonlinear Schrödinger equation using exponential integrators. *Modeling, Identification and Control*, 27(4), 2006.
- [7] H. Berland, B. Skaflestad, and W. M. Wright. Expint — A Matlab package for exponential integrators. *ACM Trans. on Math. Soft.*, 2006. To appear.
- [8] H. Berland, B. Skaflestad, and W. M. Wright. Scaling and squaring of φ functions in exponential integrators. In preparation, 2006.
- [9] S. Blanes and P. C. Moan. Practical symplectic partitioned Runge–Kutta and Runge–Kutta–Nyström methods. *J. Comput. Appl. Math.*, 142(2):313–330, 2002.
- [10] T. J. Bridges and S. Reich. Multi-symplectic integrators: numerical schemes for Hamiltonian PDEs that conserve symplecticity. *Phys. Lett. A*, 284(4-5):184–193, 2001.
- [11] S. M. Cox and P. C. Matthews. Exponential time differencing for stiff systems. *J. Comput. Phys.*, 176(2):430–455, 2002.

- [12] N. M. Ercolani, M. G. Forest, and D. W. McLaughlin. Geometry of the modulational instability III. Homoclinic orbits. *Physica D*, 43(349), 1990.
- [13] N. M. Ercolani and D. W. McLaughlin. Toward a topological classification of integrable PDEs. In R. Devaney, H. Flaschka, W. Meyer, and T. Ratiu, editors, *MSRI Proc. Workshop on Symplectic Geometry*, 1990.
- [14] B. Fornberg. *A practical guide to pseudospectral methods*, volume 1 of *Cambridge Monographs on Applied and Computational Mathematics*. Cambridge University Press, Cambridge, 1996.
- [15] M. Hochbruck and A. Ostermann. Explicit exponential Runge–Kutta methods for semilinear parabolic problems. *SIAM J. Numer. Anal.*, 43(3):1069–1090, 2005.
- [16] A. L. Islas, D. A. Karpeev, and C. M. Schober. Geometric integrators for the nonlinear Schrödinger equation. *J. of Comp. Phys.*, 173:116–148, 2001.
- [17] A. L. Islas and C. M. Schober. On the preservation of phase space structure under multisymplectic discretization. *J. of Comp. Phys.*, 197:585–609, 2004.
- [18] A. R. Its and V. P. Kotljarov. Explicit formulas for solutions of a nonlinear schrödinger equation. *Dokl. Akad. Nauk Ukrain. SSR Ser. A*, 1051:965–968, 1976.
- [19] S. Koikari. An error analysis of the modified scaling and squaring method. Submitted to *Computers Math. Applic.*, 2005.
- [20] I. M. Krichever. Methods of algebraic geometry in the theory of nonlinear equations. *Russian Math. Surv.*, 32:185–213, 1977.
- [21] D. W. McLaughlin and E. A. Overman. Whiskered tori for integrable PDEs: chaotic behavior in near integrable PDEs. In *Surveys in applied mathematics, Vol. 1*, volume 1 of *Surveys Appl. Math.*, pages 83–203. Plenum, New York, 1995.
- [22] A. Ostermann, M. Thalhammer, and W. M. Wright. A class of explicit exponential general linear methods. *BIT*, 46(2):409–432, 2006.
- [23] G. Strang. On the construction and comparison of difference schemes. *SIAM J. Numer. Anal.*, 5:506–517, 1968.
- [24] T. R. Taha and M. J. Ablowitz. Analytical and numerical aspects of certain nonlinear evolution equations. II. Numerical, nonlinear Schrödinger equation. *J. Comput. Phys.*, 55(2):203–230, 1984.
- [25] F. D. Tappert. Numerical solutions of the Korteweg–de Vries equation and its generalizations by the split-step Fourier method. *Lect. Appl. Math. Am. Math. Soc.*, 15:215–216, 1974.
- [26] J. A. C. Weideman and B. M. Herbst. Split-step methods for the solution of the nonlinear Schrödinger equation. *SIAM J. Numer. Anal.*, 23(3):485–507, 1986.
- [27] H. Yoshida. Construction of higher order symplectic integrators. *Physics Letters A*, 150:262–268, 1990.
- [28] V. E. Zakharov and A. B. Shabat. Exact theory of two-dimensional self-focusing and one-dimensional self-modulation of waves in nonlinear media. *Ž. Èksper. Teoret. Fiz.*, 61(1):118–134, 1971.